THE JOURNAL OF PHYSICAL CHEMISTRY C

 VOLUME 111, NUMBER 30, AUGUST 2, 2007

ARTICLES

Low-Lying Exciton States Determine the Photophysics of Semiconducting Single Wall Carbon Nanotubes

Gregory D. Scholes,*,†,‡ Sergei Tretiak,§ Timothy J. McDonald,†,|| Wyatt K. Metzger,† Chaiwat Engtrakul,† Garry Rumbles,† and Michael J. Heben†

[a] National Renewable Energy Laboratory, MS 3216, 1617 Cole Boulevard, Golden, Colorado 80401-3393, [b] Department of Chemistry, 80 St. George Street, Institute for Optical Sciences, and Centre for Quantum Information and Quantum Control, University of Toronto, Toronto, Ontario M5S 3H6 Canada, [c] Theoretical Division, Center for Nonlinear Studies (CNLS) and Center for Integrated Nanotechnologies (CINT), Los Alamos National Laboratory, Los Alamos, New Mexico 87545, [d] Department of Applied Physics, Columbia University, New York, New York 10027

Received: December 12, 2006; In Final Form: May 5, 2007

A combined experimental and theoretical study of the photophysical properties and excited-state dynamics of semiconducting single-wall carbon nanotubes (SWNTs) is reported. Steady-state and time-resolved fluorescence data as a function of temperature are explained on the basis of a manifold of four low-lying singlet exciton states with kinetically controlled interconversion. Relaxation among these levels is slow and therefore Kasha's rule is not obeyed. Quantum chemical calculations based on time-dependent density functional theory complement the experimental findings. The temperature-dependence of the radiative and nonradiative rate constants are examined.

1. Introduction

The photophysics of semiconducting single wall carbon nanotubes (SWNTs) have been studied intensively in recent years.[1−11] It has emerged that the lowest energy excited states are strongly bound excitons, with transition energies determined by the SWNT diameter.[12−17] The challenges to elucidating details of the excited-state dynamics that are characteristic of SWNTs are twofold. First, sample preparation is complicated and even the highest quality samples are difficult to study owing to inhomogeneous distributions of SWNTs in the ensemble. Second, models for describing the photophysics sit at the convergence of solid-state physics and molecular spectroscopy. For example, in a typical solid-state picture, electrons and holes formed by photoexcitation are unbound, and therefore, the strong binding of excitons comes as a surprise. As a further consequence of the assumption that two-electron integrals involving electron and hole configurations are small, excited states are not spin eigenfunctions. On the other hand, it is well-known that singlet and triplet states determine the spectroscopy of molecules; the approximate splitting between these states is known, and the mechanisms for their interconversion are well-studied. Obtaining a clear picture of SWNT photophysics has required a union of these viewpoints.

The optically allowed (bright) E_{11} and E_{22} states have been a focus of investigation to this point. Quantum chemical calculations suggest that the lowest lying excited-state for all tube types is an optically forbidden (dark) exciton,[13,18,19] and that conclusion has been used to rationalize the very low estimated fluorescence quantum yield of the material[20] ($\Phi_f \sim$

* Corresponding author.
† National Renewable Energy Laboratory.
‡ University of Toronto.
§ Los Alamos National Laboratory.
|| Columbia University.

10.1021/jp068541j CCC: $37.00
Published on Web 06/22/2007

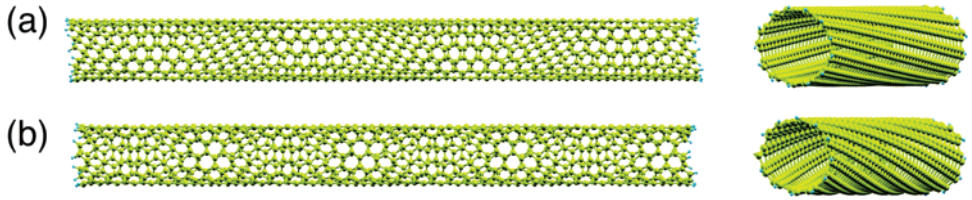

Figure 1. Structures of the two SWNTs used for the quantum chemical calculations reported in this work: (a) (7,6) SWNT and (b) (7,5) SWNT. The ends of each structure are capped with bonds to hydrogen atoms.

$10^{-3}-10^{-4}$). However, a detailed model also explaining the temperature-dependence of Φ_f and the fluorescence decay kinetics has not yet been elucidated. In other words, open questions include the following: What are the important nonradiative decay routes for the excitons, and is intersystem crossing important? In the present report, we suggest, on the basis of a combination of theory and experiment, ingredients that should be considered as researchers assemble such a model. We report an analysis of both time and frequency domain observations as a function of temperature. Examining this breadth of data imposes constraints on the analysis, which has enabled us to build on the recent reports highlighting the strong binding of excitons and the complexity of fluorescence decay kinetics. We conclude that the observed experimental trends are caused by the kinetic interplay of low-lying states.

A key component in current theories is the assumption of a Boltzmann distribution of population among the singlet states. That supposition is similar to Kasha's rule for molecular photophysics,[21,22] which states that only the lowest energy singlet state of a molecule is fluorescent. This rule is followed when the rates of internal conversion (IC) from higher excited states (e.g., S_n) to the lowest excited state (e.g., S_1) of any spin multiplicity and intramolecular vibrational relaxation (IVR) within each electronic state are much greater than the rate of deactivation of the lowest excited state (e.g., the fluorescence rate). Here, we report a detailed analysis of recently reported dual fluorescence features[23] from surfactant-isolated SWNTs that enables us to propose a basic scheme that serves as a foundation for explaining the known photophysical data for SWNTs. Our major conclusion is that the relative population of each low-lying exciton state is controlled by the kinetics of radiationless transitions between the states in competition with radiative decay channels. In other words, among the manifold of electronic excited states close to the E_{11} energy, Kasha's rule is not obeyed. This result has significant consequences for interpreting the photophysics, particularly the fluorescence decay kinetics and understanding the cause of the low fluorescence quantum yield.

2. Methods

High-pressure carbon monoxide decomposition (HiPco) SWNTs (Carbon Nanotechnologies, Inc.) were suspended in sodium dodecylbenzene sulfonate by cup−horn sonication for 12 min with a Cole Parmer 750 W homogenizer at 30% power and then sonicated overnight in a Branson 2510 ultrasonic bath. A 100% power cup−horn sonication (12 min) was followed immediately by 4 h of ultracentrifugation at 122 000 g to remove large bundles from the suspension. Eastman *AQ55* polymer (a thermoplastic, ionic polyester) dispersed in ethanol was added to the SWNT suspension, and the mixture was stirred and lyophilized to create a powder.[24]

Photoluminescence excitation spectra were obtained with a customized Thermo-Electron FT960 Raman system.[25] The excitation source for the Raman spectrometer was replaced with a 250 W tungsten halogen bulb and a single-grating monochromator, permitting continuously variable excitation from 400 to 1100 nm. The Ge detector, operated at 77 K, responded to wavelengths between 900 and 1700 nm. The system was corrected for variations in excitation intensity as a function of wavelength and for the response of the collection optics and detector. The time-resolved fluorescence data, reported elsewhere,[23] were measured using time-correlated single photon counting with low excitation intensities that minimize the complication of exciton−exciton annihilation effects.[26] A 250 kHz pulse train was focused onto a cuvette containing the SWNT sample. We estimate that there were $\sim 5 \times 10^{12}$ photons in each laser pulse. Comparing our excitation and sample conditions to those in the report of Ellingson et al.,[27] we estimate that there is approximately one exciton per 100 nm of SWNT. It is noted that annihilation effects do not influence the relative intensities of the two fluorescence bands we observe, according to our model.

Quantum chemical calculations[28] were carried out using hybrid time-dependent density functional theory (TDDFT). B3LYP (20% of HF exchange)[29] and PBE1PBE (25% of HF exchange)[30] functionals were used for the calculations. It is critical to account for excited-state electronic correlations to reproduce excitonic effects in SWNTs. The hybrid TD−DFT technique allows one to account for excitonic phenomena because of the long-range fraction of the orbital exchange.[31,32] For example, previous work has established that B3LYP and PBE1PBE kernels provide a good description of neutral excitons, both singlets and triplets, in conjugated polymers and carbon nanotubes.[31,33−36] In the case of SWNTs, both these functionals predict the known ordering of exciton states, where the dark state lies below the bright state.

Two SWNTs were investigated, as shown in Figure 1. Each tube has a finite size and is capped with hydrogen atoms. The first is a (7,6) SWNT consisting of two repeat units, ∼1000 atoms, and is ∼10 nm in length. The second is a (7,5) SWNT, also consisting of two repeat units, it contains ∼900 atoms, and is ∼9 nm in length. One needs to compromise between sophistication of the quantum chemical methodology and the size of the system studied. Hence, in the present work, we have investigated finite size SWNTs. To help to ensure that our calculations reproduce the basic properties of longer SWNTs and that they are consistent with the infinite-size limit, we chose SWNT lengths as long as feasible compared to the characteristic exciton sizes. The reasoning behind this is that once the molecular size becomes larger than the exciton size, properties saturate, meaning, for example, that the excitation energy of the lowest state in a band is unchanged with increasing length. Calculations of conjugated oligomers provide a standard example of such an approach.[37−39] Recently, more and more studies are using this technique for carbon nanotubes.[7,13,35,36,40−42]

Three basis sets (STO-3G, 3-21G, and 6-31G) were empoyed to calculate the lowest 10 singlet excitations in each SWNT. The effect of the basis set was found primarily to red shift excitation energies and did not change the qualitative picture

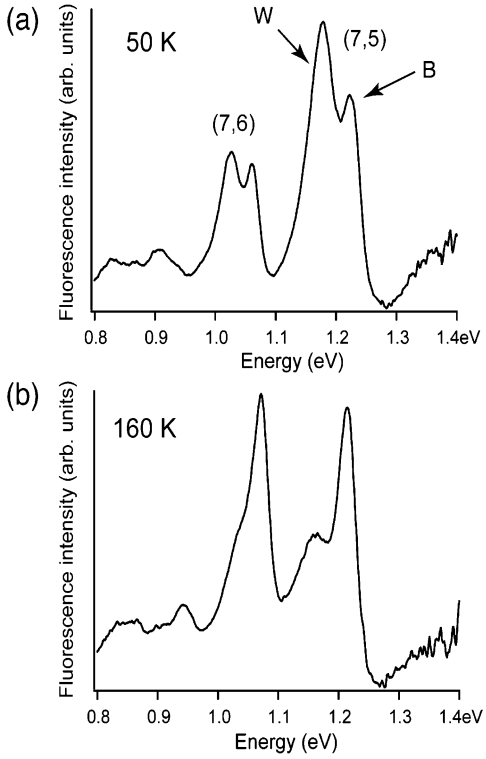

Figure 2. Slice through a two-dimensional excitation−emission plot where the excitation light is resonant with the E_{22} transition of the (7,5) SWNT at (a) 50 K and (b) 160 K. The spectra indicate that emission from the (7,6) SWNT is also observed at the (7,5) excitation wavelength, but the emission is well-separated from that attributed to the (7,5) SWNT. Related contour plots for 298 and 4 K are reported in ref 23.

obtained of the electronic states. The differences between the results obtained using 3-21G and those obtained using 6-31G basis sets were found to be insignificant. Using basis sets augmented by polarized and diffuse functions would lead to further very small red shifts, as evidenced in calculations of smaller tubes (not shown). Consequently, large basis sets are not essential for calculating electronic excitations in semiconducting carbon nanotubes, and we find that the STO-3G level is sufficient to present a useful qualitative picture.

3. SWNT Fluorescence

It is now well-known that the fluorescence emission spectra of individual SWNT types within a sample ensemble can be identified by recording emission spectra as a function of excitation wavelength.[2] In recent work, we reported steady state and time-resolved fluorescence measurements of a sample of semiconducting SWNTs and concluded that multiple emitting electronic states can be observed.[23] For example, Figure 2 displays a slice through an excitation−emission plot where the excitation light is resonant with the E_{22} transition of the (7,5) SWNT for two different temperatures. The plot indicates that emission from the (7,6) SWNT is also observed at this excitation wavelength, but it is well-separated from that attributed to the (7,5) SWNT. At 300 K (not shown), one emission band attributed to the bright exciton (labeled B) is seen at ~1.2 eV for the (7,5) SWNT. Notably, as the temperature is lowered, a low-energy shoulder (labeled W) accompanies the main emission band. At 50 K (and below), that spectral feature dominates the emission spectrum of the (7,5) SWNT.

We observed the appearance of a clear shoulder corresponding to the W band for the (7,5), (7,6), (8,4), (8,6), and (9,5) SWNT emission spectra in the present sample. However, this does not mean that other tube types do not show the shoulder, since it may be difficult to resolve when emission spectra of different tube types overlap, as is often the case. The focus of this paper is to discuss the origin of this emission feature and to explain how it participates in the SWNT photophysics. We focus only on the (7,5) and the (7,6) SWNT data, which we present in the following sections.

A first point to note is that W is apparently not a vibronic feature associated with the electronic transition B. This was determined experimentally in ref 23 and is corroborated by theoretical arguments. Indeed, the low-energy fluorescence band, that we refer to as W, is separated from the room-temperature feature, B, by an energy similar to that corresponding to the radial breathing mode frequency.[43] However, it is clear that W cannot be attributed to a phonon side band because such an assignment requires the Huang−Rhys factor[41,42] to be temperature dependent. Physically, this is unlikely in any molecular system, unless it undergoes a temperature-dependent conformational change, because chemical bonds are substantially stronger than normal thermal energies. The possibility of temperature-dependent Huang−Rhys factors has been discussed in the context of conjugated polymers;[44] however, extensive theoretical modeling of similar data in our laboratory suggests that caution should be exercised when applying few-mode fitting models, particularly when torsional modes are important. See, for example, ref 45. Note that our simulations do include the vibronic band associated with the radial breathing mode, and we find that this band plays a significant role in shifting the apparent W band peak as a function of temperature. Thus, we find that the overall features of the spectrum require both W and the vibronic band associated with B.

4. Quantum Chemical Calculations

In order to obtain insight into the electronic states and their oscillator strengths, we performed extensive quantum chemical calculations using TDDFT, as described above. Previous high quality quantum chemical calculations have established a basic picture for the lowest energy excited states of SWNTs, wherein the lowest electronic state is dark and the bright state B always lies higher in energy.[7,13,18,36] Other states have been predicted that lie slightly above or below the bright exciton (all higher in energy than the dark exciton), but the precise positions of these bands and their role in photophysical processes is unknown at this time. It is the goal of the present work to explore these states further. The quantum chemical calculations we report here complement previous theoretical studies of SWNT exciton states, in particular, since fewer calculations have been reported for chiral SWNT than zigzag SWNTs.

The magnitude of the B−D energy splitting has been predicted to be dependent on the SWNT diameter.[46] With respect to comparing theory to experiment, it is known that the absolute calculated magnitudes (but not trends) of those splittings are likely to depend on the quantum chemical methodology.[47−49] It will particularly depend on the treatment of electron correlation beyond that included in the Hartree−Fock approach, as well-documented in the literature.[50,51] With uncertainty in calculated transition energies of ~0.5 eV, experimental input, guided by calculations, is needed to determine the absolute spacing of the bright and dark exciton states.

The results of our calculations are collected in Table 1. To interpret these results and relate them to the SWNT one-dimensional exciton, we recall that each exciton forms a band owing to the periodicity of the wave function along the SWNT

TABLE 1: Calculated Excitation Energies (eV) and Oscillator Strengths (in Parentheses) for the SWNTs Using the TD−DFT Technique

SWNT	state[a] (band)	B3LYP STO-3G	B3LYP 3-21G	B3LYP 6-31G	PBE1PBE STO-3G	PBE1PBE 3-21G	PBE1PBE 6-31G
(7,6) 2 units	1 (I)	1.285 (0.0)	1.162 (0.0)	1.151 (0.0)	1.366 (0.0)	1.227 (0.0)	1.216 (0.0)
	2 (II)	1.307 (0.001)	1.183 (0.007)	1.174 (0.01)	1.392 (0.001)	1.249 (0.01)	1.235 (0.01)
	3 (III)	1.307 (0.0)	1.184 (0.0)	1.174 (0.0)	1.393 (0.0)	1.250 (0.0)	1.250 (0.0)
	4 (I)	1.354 (0.27)	1.222 (0.28)	1.208 (0.31)	1.437 (0.24)	1.288 (0.25)	1.236 (0.31)
	5 (II)	1.375 (0.76)	1.245 (0.81)	1.226 (0.84)	1.463 (1.35)	1.308 (1.45)	1.274 (1.53)
	6 (III)	1.380 (0.0)	1.249 (0.0)	1.228 (0.0)	1.468 (0.0)	1.312 (0.0)	1.288 (0.0)
	7 (IV)	1.392 (13.29)	1.257 (14.3)	1.243 (14.0)	1.481 (15.0)	1.330 (15.7)	1.297 (15.1)
	8 (I)	1.451 (0.0)	1.315 (0.0)	1.312 (0.0)	1.538 (0.0)	1.382 (0.0)	1.387 (0.0)
(7,5) 2 units	1 (I)	1.374 (0.0)	1.262 (0.0)	1.238 (0.0)	1.457 (0.0)	1.328 (0.0)	1.303 (0.0)
	2 (II)	1.399 (0.001)	1.286 (0.021)	1.257 (0.027)	1.489 (0.26)	1.358 (0.4)	1.332 (0.41)
	3 (III)	1.401 (0.0)	1.288 (0.0)	1.258 (0.0)	1.490 (0.0)	1.359 (0.0)	1.332 (0.0)
	4 (I)	1.429 (0.32)	1.306 (0.64)	1.275 (0.52)	1.515 (0.105)	1.375 (0.13)	1.378 (0.11)
	5 (II)	1.458 (1.4)	1.335 (1.6)	1.307 (1.8)	1.550 (2.3)	1.411 (1.7)	1.396 (1.9)
	6 (III)	1.459 (0.0)	1.337 (0.0)	1.308 (0.0)	1.550 (0.0)	1.410 (0.0)	1.394 (0.0)
	7 (IV)	1.478 (12.4)	1.364 (12.7)	1.350 (12.8)	1.570 (10.5)	1.441 (11.0)	1.421 (10.9)
	8 (I)	1.508 (0.0)	1.381 (0.0)	1.367 (0.0)	1.598 (0.0)	1.453 (0.0)	1.461 (0.0)

[a] States are numbered in order of increasing transition energy. The band label groups the states calculated for the finite length SWNT into the coresponding exciton band. Thus, the lowest (dark) exciton band (D) is labeled I, while the lowest bright exciton band (B) is labeled IV. We refer to bands II and III as W and N.

long axis. However, our TDDFT calculations are only feasible for finite SWNT lengths, so quantum confinement is introduced. This leads to the calculation of a ladder of levels for each exciton state rather than a continuous band. This strategy is the same as that employed by Mazumdar and co-workers.[13,52] To some extent, this picture may even be realistic because, through exciton−nuclear coupling, the exciton in "real" SWNTs can be localized depending upon sample preparation, average tube length, inhomogeneity of the local dielectric environment, defects, intertube interactions, and exciton−phonon coupling. Detailed considerations of these effects are beyond the scope of the present work. The main result communicated by Table 1 is that there is seen to be three exciton bands below the bright state, and the relative energetic ordering of those states can be calculated.

A characteristic standing wave structure[31,53] is seen in the transition densities plotted in a real-space representation for each state, Figure 3a, and it enables us to assign each band. For example, four bands are seen with their lowest states ($k = 0$ in an infinite system) being numbers 1−3 and 7 in Figure 3a. The standing waves for the next states in each band have two nodes, for example, numbers 4−6 and 8. We label each exciton band I, II, III, and IV, as indicated in Figure 3b and Table 1. The lowest state in each exciton band is important, while the density of states in each exciton band will increase as the SWNT length approaches infinity. According to the model of Zhao et al.,[13] two near-degenerate pairs of highest occupied molecular orbitals and lowest unoccupied molecular orbitals (HOMO−LUMO) give rise to four excitonic bands, here labeled as the exciton bands I−IV. Only the exciton state IV is optically allowed because of specific Coulomb interactions and electronic correlations. Our calculations are fully consistent with this picture (Table 1).

The bright state B is clearly evident (exciton state IV), and there are three nominally dark exciton bands below B in energy (I−III). We label these states D, W, and N in order of increasing transition energy, and we discuss below the way they may participate in SWNT photophysics. Figure 3 shows the diagonal elements of the 5056 × 5056 transition density matrix calculated with the STO-3G/TD-B3LYP method (a basis set size of 5056). Typically, transition densities are highly oscillating according to the nodal structure of the wave functions involved, as is evident in these plots. Inspection of Figure 3a reveals that the completely forbidden states have symmetric transition densities over the direction of the transition dipole. On the other hand, each allowed transition has a nonzero transition dipole that necessarily introduces an asymmetry in the shape of the transition density plot. An analogy with A_g (dark) and B_u (bright) states in conjugated polymers[54] corroborates these trends. A notable result is that some of the states in the dark exciton bands are calculated to be weakly optically allowed. These allowed states include the nonzero momentum states of the dark excitons forming standing waves along the tubes. Figure 3a shows that the asymmetry and consequently the oscillator strengths of these transitions are coming from the middle part of the tube and not from the ends. Such weakly allowed states are not found in computations of selected zigzag tubes using our methods (data not shown). Thus, it is possible that the chirality (or deviation from zigzag) of the tube in concert with finite length effects (or end effects) plays a role in enabling these states to be weakly optically allowed. These states are expected to be completely forbidden in infinite-sized SWNTs on the basis of the selection rules,[55] but evidently, that is not the case for the TDDFT calculations of finite size SWNTs. In chiral tubes, the $k = 1$ (II, III band) exciton gains the weak oscillator strength from the spatially localized place where the wave function has a node. This is not an artifact of the ends. Note, though, that the $k = 2$ state is completely forbidden since the effects of the pair of nodes cancel each other. For related reasons, in the infinite tube limit, the ratio of the oscillator strength between the weak state $k = 1$ (II, III band) and bright state $k = 0$ (IV band) goes to 0, just as expected. Though this result is worthy of future examination, we do not rely on it for the interpretation of the experimental data.

At this point, we invoke the analysis of excited states in terms of natural transition orbitals (NTO),[56] which provides the best representation of the excited states in terms of single-particle transitions. Each calculated state can be represented by two pairs of NTOs, each capturing about 50% of the state character. These pairs are very similar, and only one pair is shown for each state in question for the (7,6) tube in Figure 4. The first dark state, 1, and bright state, 7, are transitions between delocalized electron and hole states, similar to what has been observed in conjugated polymers.[37] The weakly allowed state W (5) has an electron orbital that appears very similar to those of states 1 and 7. The hole orbital has a single node, which points to nonzero momentum. Looking at all of the orbitals, we see that they are spiraling around the tube, following the chirality.

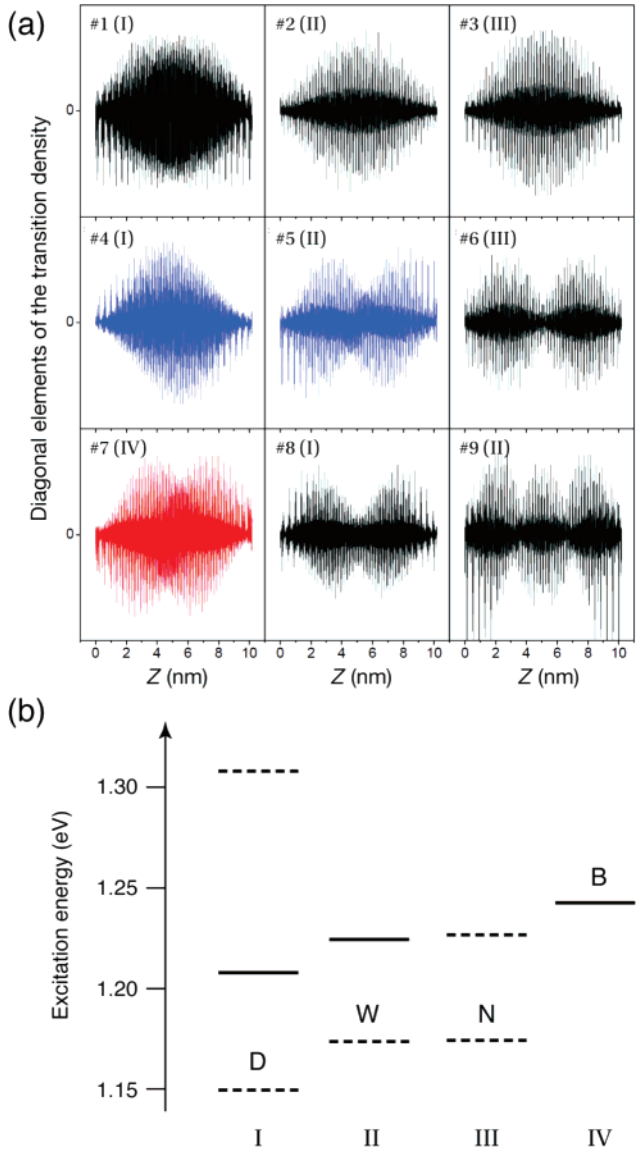

Figure 3. (a) Plots of the diagonal transition density matrix elements calculated at the STO-3G/TD-B3LYP level as a function of position along the length, *Z*, of the finite-sized (7,6) tube. Transition densities from the ground state to each excited state #1−9 (see Table 1), as indicated on the plots, is shown. The forbidden transitions are plotted in black, the weakly allowed transitions are in blue, and the bright state transition is in red. The allowedness of transition #7 is evident by the transition density having a dipole (transition) moment along *Z*. (b) Diagram showing the order of states for the (7,6) SWNT and band assignments (B3LYP/6-31G calculation of a finite length SWNT). Our labels (D, W, N, and B) are used to describe the photophysics.

Our electronic structure calculations suggest that exciton states below the bright exciton can gain oscillator strength in short chiral SWNTs and that these states associated with dark exciton manifolds might explain why the W state is observed for our SWNT sample preparation. On the other hand, any one of the dark exciton states may gain intensity through a coupling to vibrational motion or via symmetry breaking.[57] The difficulties encountered when examining these hypotheses include the following: (i) we can only resolve the shoulder clearly on five SWNTs in the presently available data, (7,5), (7,6), (8,4), (8,6), and (9,5), because of the problem of overlapping spectra; and (ii) on the basis of these experiments, we can only be confident in assigning B. To analyze the experimental data, we rely on theory only to suggest that there are four low-lying exciton states that should be considered and that the lowest is the dark state D, while the highest energy state is the bright state B. Our goal is to try to identify the positions of the states and to decide how the states might participate in photophysical dynamics governing fluorescence decay profiles and quantum yields.

6. Simulations and Models

In this section, we describe the methodology we have used to model the photophysics of the SWNTs. We aimed to employ a model that would enable a realistic calculation of the steady-state fluorescence and the time-resolved fluorescence as a function of temperature. Hence, it is important not to constrain the model to a fast relaxation limit (i.e., Boltzmann populations of the states). While undertaking this work, many permutations were explored, and we attempted to decide what minimal models were consistent with experimental observations. It was found that, while many levels could be (and were) included in the modeling, useful physical insights could be ascertained by considering effective two-level or three-level systems (e.g., containing the observed or rate-determining states).

From a spectroscopic point of view, a first step toward understanding the origin of the two bands in the SWNT emission spectra is to consider the possibility that the lower energy band W is, in fact, the dark state (i.e., D), made allowed through vibronic coupling or intensity borrowing via Coulomb interactions. Symmetry breaking can only realistically lead to an allowed lower exciton state if the circular symmetry of the wave function is disrupted or lowered.[58] In SWNTs, a related effect has been observed in the presence of magnetic fields, leading to an Aharonov−Bohm effect that alters the wave function periodicity through a circumferential boundary condition.[57,59] It is possible that a related effect, perhaps even a chemical modification, can lower the symmetry to allow one of the dark states to borrow oscillator strength from B. Indeed, in the model proposed by Mortimer and Nicholas, it is assumed that a dark state can borrow substantial intensity from B (up to 20%).[60]

In the case of vibronic coupling,[41,42] a band may be observed in emission as a result of Herzberg−Teller coupling.[61] In that case, we would be observing an energy band at the energy of the dark exciton state minus the energy of the vibration that has appropriate symmetry to allow borrowing of intensity from the bright state. In that case, W would represent a false origin.[61−63] The symmetry of the required vibrational mode for the SWNT is such that it is neither IR nor Raman active,[64] so we cannot estimate the frequency. Even so, the absence of a distinct vibronic progression associated with W suggests that if Herzberg−Teller coupling enables intensity borrowing, then the active mode has a low frequency. In the case of intensity borrowing from a third body,[65] for example, surfactant or another SWNT in the micelle, the position of W would be approximately equal to the energy of the dark state. Such effects are unusual, but possible. In the simulations reported below, we assume that, if W represents a false origin, it is closely located to the parent dark state.

Through iterative analysis of the temperature-dependent emission spectra, we conclude that a two-level model can adequately describe some of the data if the oscillator strength of W is much less than that of B. This model does not preclude the existence of other electronic states between B and W but suggests that such states (if present) are not significant in terms of their influence on the fluorescence emission spectra. In the limit that the radiationless transition rates $k_{m\leftrightarrow n}$ connecting the two levels are fast relative to the radiative rates (the high-temperature limit), a Boltzmann distribution of population

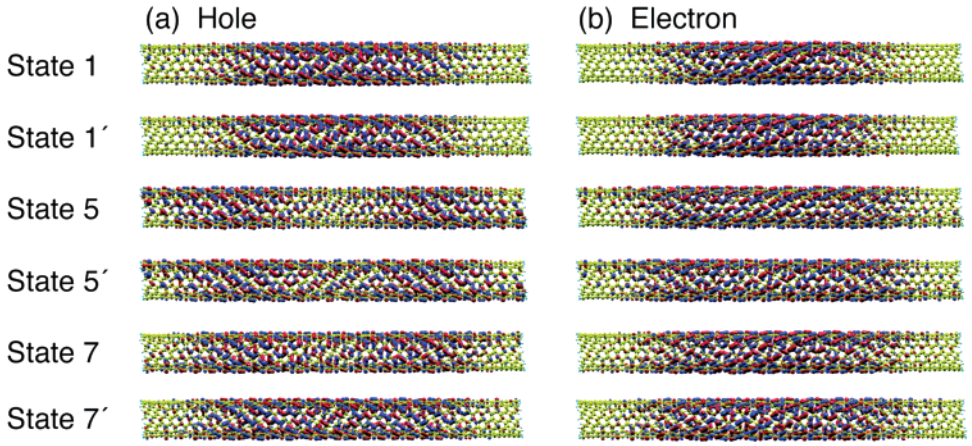

Figure 4. Natural transition orbitals (NTOs) for the (7,6) SWNT calculated at the STO-3G/TD-B3LYP level. These plots should be interpreted as follows : First, through the NTO analysis[56] each SWNT transition is found to be a linear combination of two excitations, as described previously by Zhao and Mazumdar.[13] We label these #*N* and #*N*′. Second, the natural transition orbital analysis allows us to define a simple orbital-type representation of the electronic transition density matrix. The "electron" transition orbital is the density associated with the excited electron density (i.e., the upper unoccupied molecular orbitals involved in the transition), while the "hole" transition orbital shows the shape of the density occupied by that excited electron density in the ground state.

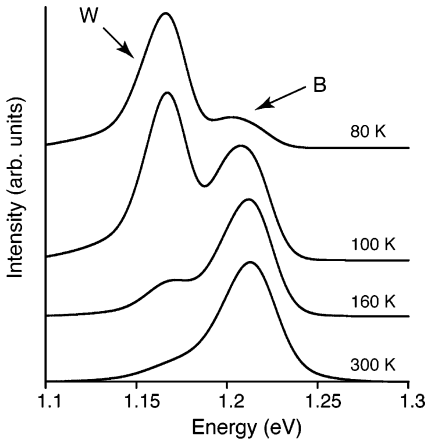

Figure 5. Simulations of the fluorescence emission spectra for the (7,5) SWNT based on a two-level model with excited states W and B. Here, it is assumed that there is fast equilibration of population among the states to arrive at a Boltzmann population distribution prior to emission. This is the type of model usually assumed in the literature up to this point.

among the levels is attained prior to emission. That is the model assumed in most previous reports and is consistent with Kasha's rule. Assuming this approximation holds, we can simulate the fluorescence data between 300 K and about 100 K with the two-level model, but below 100 K, we find the emission spectrum to be overwhelmingly dominated by the W band, Figure 5, which is inconsistent with our experimental observations.

Thus, the basic model needs refinement. Specifically, it is necessary to remove the assumption of fast relaxation between levels (leading to the Boltzmann population distribution). Instead, we explicitly model the rates of relaxation among the SWNT exciton bands, as shown in Figure 6. In our simulations of the time and frequency-resolved spectroscopy, it is assumed that B and W are populated equally rapidly after photoexcitation of the upper, E_{22} band. That presumably occurs in competition with alternative internal conversion pathways. This assumption is reasonable, but it can be relaxed without altering our conclusions. We also assume that exciton−exciton annihilation, if it occurs, happens faster than relaxation dynamics among the lower exciton states. The subsequent population dynamics were modeled numerically by solving the Pauli master equations,[66]

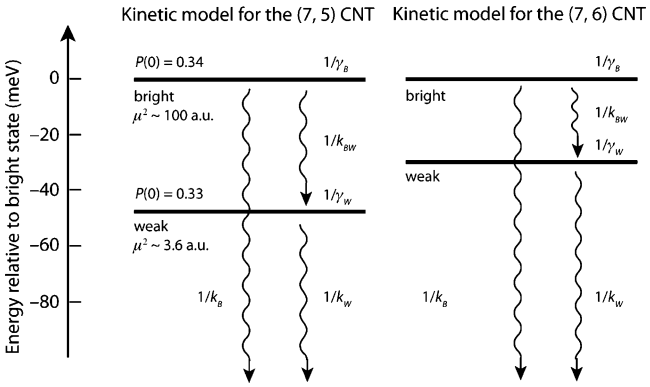

Figure 6. Three-level model showing the bright (B) and weak (W) levels. If dark state (D) is also included in the simulations, we find that it must lie sufficiently below the bright state (∼100 meV) and that its precise position cannot be ascertained. Ultrafast relaxation processes may be involved in determinng the initial population distribution among these states after excitation of the E_{22} transition, but it is unecessary to include them to model the dual peaks in the fluorescence emission.

$$\frac{dP_m(t)}{dt} = -\gamma_m P_m(t) + \sum_n (k_{n\to m} P_n(t) - k_{m\to n} P_m(t)) \quad (1a)$$

$$\frac{dP'_m(t)}{dt} = \gamma_m P_m(t) \quad (1b)$$

where P_m is the population density of electronic state m, γ_m is the radiative decay rate, k_{m-n} are the rates of population relaxation among the states. The $P'_m(t)$ are the ground state populations produced by radiative emission from each state. They define the time-resolved emission and quantum yield associated with each state.

Each reverse (uphill) rate is determined according to detailed balance, where ΔE_{12} is the energy difference between the states and k is the Boltzmann constant:

$$k_{2\to 1} = k_{1\to 2} \exp(-\Delta E_{12}/kT) \quad (2)$$

The temperature dependence of each radiationless transition rate[67,68] is assumed to follow the usual form of the temperature-dependence of nonradiative transitions that we assume holds

reasonably well for SWNTs,

$$k_{m\rightarrow n} = k^0 + B_k \exp(-\theta_k/kT) \quad (3)$$

where we find from our simulations that $\theta_k \approx 5$ K, $k^0 \sim 1$ ns^{-1}, and B_k is chosen so that the values we report for the rate constants $k_{m\rightarrow n}$ apply to $T = 300$ K. For example, if we quote $k = 0.005$ ps^{-1}, then $B_k = (0.005 - 0.001)/\exp(-5/300) = 0.0041$. The consequences of temperature-dependent nonradiative transitions are examined in section 7.

The difficulty with analyzing the temperature dependence of SWNT photophysical observables is that both the nonradiative and radiative rate constants vary with temperature, in contrast to molecules where all of the temperature dependence can be attributed to the nonradiative processes. The radiative rate of state B is temperature-dependent because the exciton band IV in fact consists of a ladder of states, where the lowest state can radiate but the upper states are dark. For a SWNT of infinite length, those upper states are dark owing to the requirement of momentum conservation for exciton recombination. Thermal population of this ladder of states therefore lengthens the effective radiative rate of B because it is controlled by the population of the lowest level in the band. This complication in the photophysics of SWNTs, that the radiative decay rate depends on temperature, is common to molecular aggregates, such as J aggregates.[69−71]

To account for this thermal occupation of exciton states away from the zero momentum exciton state,[18,72] we consider the effective decay rates to be governed by as suggested by Spataru

$$\gamma_m = \gamma_m^0 \sqrt{\theta_g/kT} \quad (4)$$

et al.,[18] where γ_m^0 is the $T = 0$ K radiative decay rate and we take $\theta_g \sim 0.37$ μeV. This functional form of the effective radiative rate strictly applies to an infinite length SWNT only, assuming a parabolic exciton band. Nonetheless, we assume that it captures reasonably well the temperature-dependence of both the B and the W radiative decay rates. Using the expression for γ_m in our simulations, we find that the bright state has a radiative time constant of 12 ps or 25 ps (depending on the simulation) at 0 K, leading to a radiative decay time of at least 1 ns at 300 K. The 0 K radiative rate is fast, as found from calculations,[18] because of the collective, superradiant nature of the emission. We will discuss this temperature dependence further below.

Fluorescence spectra were calculated using the expression[73]

$$\sigma_F(\omega) \propto \sum_m P'_m \frac{\omega^3}{n} F_E(\omega) \quad (5)$$

where n is the solvent refractive index and P'_m is the total radiated population from electronic state m obtained via eq 1 as $\int_0^\infty dt P'_m(t)$. The line shape function is given by

$$F_E(\omega) = \frac{1}{\pi}\sum_k B_k \mathrm{Re}\int_0^\infty dt \langle k(0)|k(t)\rangle \exp[i(\omega - \omega_{0m} + \omega_k + \lambda_m/\hbar)t - g^*(t) - {}^1/_2\sigma^2 t^2] \quad (6)$$

where k labels the vibrational modes of the excited state. The Franck−Condon factors for absorption and emission are evaluated in the time domain, as described elsewhere.[73] B_j are the Boltzmann populations of these levels, which have frequencies ω_j, and $\omega_{0m} = E_{0m}/\eta$ is the ground to excited state frequency gap. We consider modes of frequency 17, 117, and 1500 cm^{-1} and the SWNT type-dependent radial breathing mode. The reorganization energy is λ_m (half the Stokes shift); σ is the standard deviation of the Gaussian distribution of static disorder in the electronic energy gaps, and $g(t)$ is the homogeneous line shape function. This line shape function incorporates an explicit temperature dependence.[74−77] The asterisk indicates the complex conjugate. We use a single overdamped Brownian oscillator[74] with reorganization energy 50 cm^{-1} and modulation frequency 1000 cm^{-1} to model the homogeneous line shape, but we find that the spectral line shape is dominated by inhomogeneous broadening.

Interestingly, for the present samples, we find that the inhomogeneous line broadening in the (7,5) spectrum, $\sigma = 110$ cm^{-1}, is substantially larger than that for the (7,6) SWNT, where we find $\sigma = 80$ cm^{-1}. This inhomogeneous broadening, which is characteristically evident as temperature-independent line shapes,[75] may reflect deformations and strains on the SWNT, as well as the influence of local environment.[78] The homogeneous contribution to line broadening, caused by exciton−phonon coupling,[79] is modeled by $g(t)$ but is obscured by the inhomogeneous line broadening. However, bearing in mind the fluctuation−dissipation theorem, we infer exciton−phonon coupling to be small because the Stokes shift is small.

7. Analyses and Discussion

Here, we report results of our modeling of the SWNT photophysics. In the first part of this section, we show that the dual fluorescence feature and its temperature-dependence can be reproduced by a three-level model, where the bright state B relaxes to a weakly allowed state W, which, in turn, relaxes to the lowest dark state, D. Two important features of this model are that the thermally activated uphill process can occur and the B−W energy splitting retrieved by the model matches the splitting of the two bands in the fluorescence spectrum for each SWNT. We were able to capture the general features of the fluorescence decay kinetics but not every aspect. Specifically, we could reproduce the rate coefficients well but were unable to discover the reason for the relative amplitudes of the two dominant decay components. In the latter part of this section, we discuss a two-level kinetic model from the viewpoint of its analytical solution. In that analysis, we find evidence to support the possibility that the temperature dependence of the B fluorescence band is best explained by assuming a dark exciton state, that we label N, lies closely below B in energy (higher in energy than W). Hence, a simple two-level treatment may not be realistic, but instead all four states are likely to influence the overall photophysics. We find evidence that the temperature dependence of B emission is largely dictated by the radiative rate, which, in turn, suggests that the coherence length of the exciton is large.

7.1. Bright and Weak States. To model the origins of the dual emission features seen for several of the SWNTs, we found the model shown in Figure 6 captured the temperature dependence of the spectra. We explicitly included three levels in the model (B, W, and D) and examined the consequences of their relative spacing and ordering. However, it was decided that the results most consistent with experiment were obtained when D was lowered sufficiently that it contributed little to the observables via the uphill transfer of population (it thus serves as a population sink). We note that the model does not preclude the involvement of other states intermediate between B and W. On the basis of the three-level model, the fluorescence emission for the (7,5) and (7,6) SWNTs could be reproduced, as shown in Figure 7. The caption of that figure lists the optimized parameters used in the model. The agreement between experi-

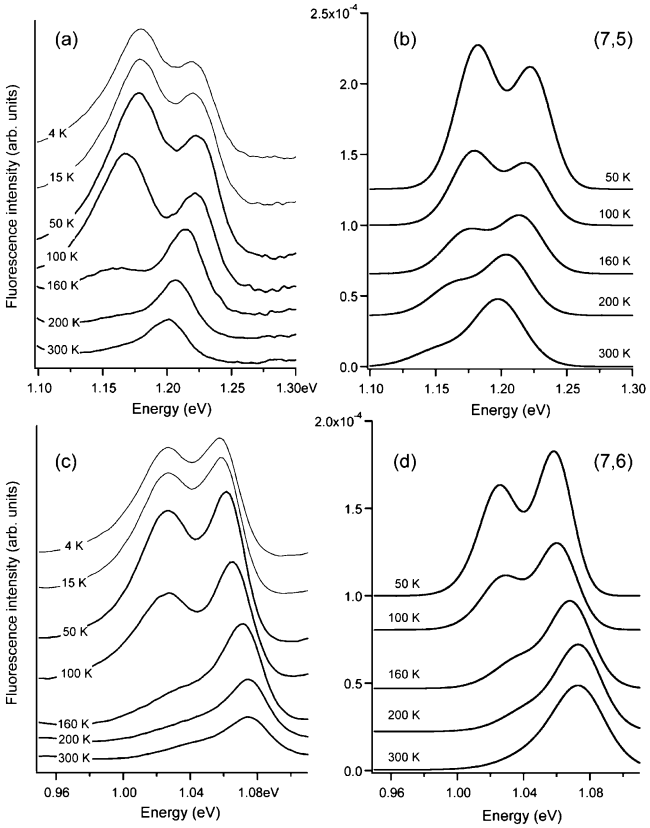

Figure 7. Experimental fluorescence emission data (emission slices through the excitation−emission plots, see Figure 1) for (a) the (7,5) SWNT and (c) the (7,6) SWNT. The corresponding simulated spectra for temperatures 300 to 50 K are shown in b and d, respectively. See text for details. The two emission peaks seen at low temperatures provide evidence that the radiative rate of B competes with population relaxation from B to the lower exciton bands. Parameters used in the simulations, based on the scheme in Figure 6, are those described in the text together with the following. (a) The (7,5) SWNT: $1/\gamma_B(0\ K) = 25$ ps, $1/\gamma_W(0\ K) = 700$ ps, $1/k_{BW} = 200$ ps, $1/k_B = 200$ ps, and $1/k_W = 3$ ns. (b) The (7,6) SWNT: $1/\gamma_B(0\ K) = 25$ ps, $1/\gamma_W(0\ K) = 1000$ ps, $1/k_{BW} = 230$ ps, $1/k_B = 230$ ps, and $1/k_W = 3$ ns.

ment and theory is reasonable: both show splitting between W and B states on the order of several tens of milli-electrovolts. This simple model predicts the fluorescence quantum yield to increase by a factor of 2 to 3 between 300 and 50 K for both SWNTs studied here. That prediction is consistent with our experimental observations. The parameters required to simulate the (7,5) and the (7,6) SWNT data are very similar, as expected. According to the model shown in Figure 6, it is the subtle differences in the energy splitting between B and W as well as slightly different internal conversion rates and radiative lifetimes that lead to the different temperature dependence of the emission band intensity profiles.

As a more stringent quantitative test of our approach, we modeled the time-resolved fluorescence. Fluorescence decays were simulated using eq 1 and by acquiring the probability of radiative emission as a function of time for each emissive species. It turned out to be very difficult to simulate both the temperature-dependent emission spectra and the fluorescence decays. A characteristic of the experimental fluorescence decay curves is the large amplitude of a ~100 ps component and a small but important contribution from a ~1 ns component.[20,80] For example, the experimental data shown in Figure 8 are fitted by the function $i_B(t) = 0.144\ \exp(-t/\tau_1) + 0.0008\ \exp(-t/\tau_2)$, with $\tau_1 = 74$ ps and $\tau_2 = 0.9$ ns. As temperature is lowered, the dominant decay time lengthens.[23] It was possible to simulate

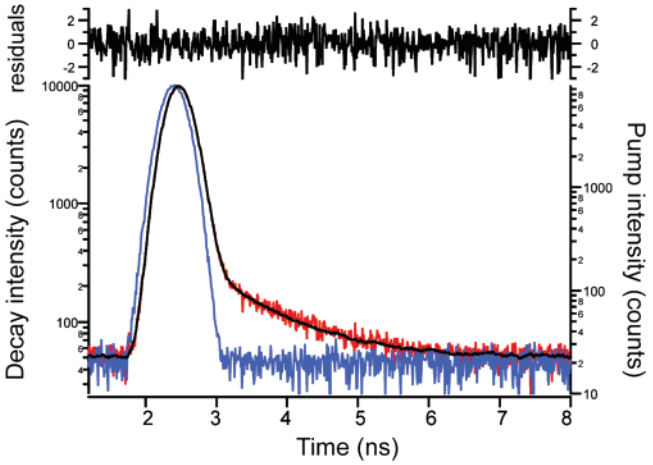

Figure 8. Experimental data and fit of the fluorescence decay for the (7,5) SWNT at 300 K. The instrument response function is shown in blue, the data are red, and the fit is the black line.

the dominant trends and exponential components for different temperatures, but to reproduce completely this decay shape at 300 K on the basis of our model while retaining the assumptions of detailed balance (eq 2), it was necessary to lower the W state to >100 meV below B, which is not considered reasonable.

Despite not being able to model all aspects of the time-resolved fluorescence, we can conclude that the fluorescence decays are largely determined by the kinetics of radiationless decay processes rather than the radiative decay rate of either electronic state. The decay rates and amplitudes obtained by analysis of the time-resolved fluorescence data are complicated functions of the rate constants input into the model. Although the kinetic scheme is well-known, interpretation of the fitting parameters is not obvious.[81,82] On the basis of the present work, it is apparent that the subnanosecond decay time is dictated by a combination of the rapid radiationless decay of B to an unspecified lower state(s) and the rate of conversion from B to W. In the steady-state spectra, the low fluorescence quantum yield results from a combination of the radiationless deactivation processes and the fact that the lowest electronic state is only weakly radiative. Its temperature dependence is attributed to the kinetically controlled depopulation of the electronic states. For example, at 300 K, $1/\gamma_B = 1$ ns for the (7,5) SWNT, while the dominant decay component is closer to the rate constant $1/k_{BW} = 100$ ps. As temperature is lowered, the effective radiative rate increases so that at 50 K $1/\gamma_B = 408$ ps, while the nonradiative rates increase. At low-temperature, we therefore expect that the fluorescence decay curves reflect more closely the radiative decay rate.

7.2. Temperature-Dependence of the Bright State. To understand better the interplay between B and a lower state, it is convenient to consider the explicit solution for a two-level kinetic scheme. Hence, the interconversion of B and another state, N, contribute to fluorescence decay curves, and the corresponding quantum yields according to:

$$i_B(t) = A_1 \exp(-\lambda_1 t) + A_2 \exp(-\lambda_2 t) \quad (7a)$$

$$i_N(t) = A_3 \exp(-\lambda_2 t) - A_3 \exp(-\lambda_1 t) \quad (7b)$$

$$\Phi_B = A_1/\lambda_1 + A_2/\lambda_2 \quad (7c)$$

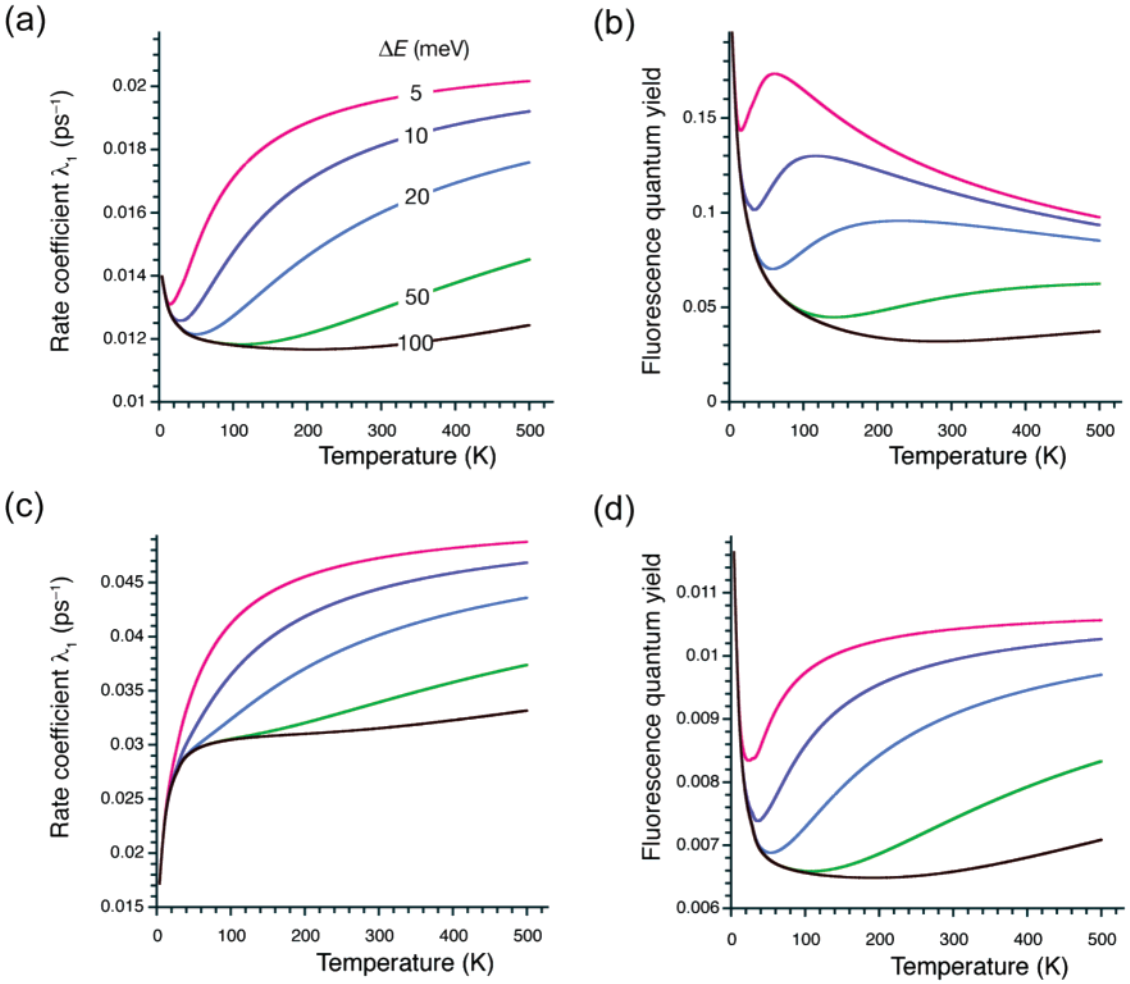

Figure 9. (a and b) Simulations based on eq 7a of the variation of the dominant decay rate coefficient (λ_1) and its relative fluorescence quantum yield (Φ_B) as a function of temperature and B−N energy difference (ΔE) assuming that only the radiative rate γ_B is temperature dependent. (c and d) As above, but assuming only the nonradiative rates are temperature dependent.

$$\Phi_N = A_3/\lambda_2 - A_3/\lambda_1 \quad (7d)$$

The explicit expressions for the rate coefficients and pre-exponential factors can be found reported elsewhere.[80,82] To gain some insight into the temperature-dependence of the radiative and nonradiative rates and to look more closely at the possible energy spacing of low-lying exciton states, we modeled the B emission, assuming the two-level model, but now as a function of the B−N energy spacing as well as temperature. In these simulations, we are focusing on the properties of B only, and N represents the most important (kinetically) lower exciton state. Therefore, N might correspond to W, or it may be another dark exciton state. Parameters similar to those reported in the caption to Figure 7 are used, but the precise values do not matter since only the trends on the curves are important for this discussion. Representative results are plotted in Figure 9. In the first set of calculations, Figure 9a,b, we assume that the dominant temperature-dependent rate constant is γ_B. Thus, the nonradiative rate constants are set to be temperature independent. In the second set of calculations, Figure 9c,d, all of the temperature dependence is attributed to the nonradiative rates ($\gamma_B = 0.0002$ ps^{-1}).

By comparing these simulations to experimentally measured emission intensities[23,60] and decay times[23] as a function of temperature, we draw the following conclusions. First, it seems most likely that the dominant temperature dependence comes from the radiative decay of B. This is particularly suggested by the form of the quantum yield of B emission versus T for small values of ΔE. The characteristic increase, then turnover to a decrease of Φ_B as temperature is lowered, is a result of the interplay between the radiative rate γ_B, which increases Φ_B as T is lowered, and the kinetic interconversion between B and N. At low temperature, the uphill transfer from N to B is "turned off", which causes the decrease of Φ_B in the lower temperature regime. The interesting corollary of that suggestion is that it means the exciton state is associated with a band, which is the currently accepted view, and it supports the theoretical model for the temperature dependence of γ_B (cf. eq 4).[18]

The second conclusion is that an important optically forbidden state lies only 5−10 meV below B. That was also concluded in a recent study by Mortimer and Nicholas using Kasha's rule and the implicit assumption that the nonradiative recombination rate was constant with temperature, which attributed that state to the lowest dark state, D.[60] Drawing on the quantum chemical results, however, we find that it is possible that such a state is not necessarily D but may be one of the other two dark states that lie below B (N or W).

7.3. Summary. We conclude that to understand the second band seen in our fluorescence spectra, we need to consider the interplay between the bright state B and the state W that lies some tens of milli-electrovolts below B. The relative positions of these states (note, that does not preclude the presence of intermediate states such as N) allows us to explain the fluorescence spectra as a function of temperature; in particular, the relative intensities of the two bands. We do not have a

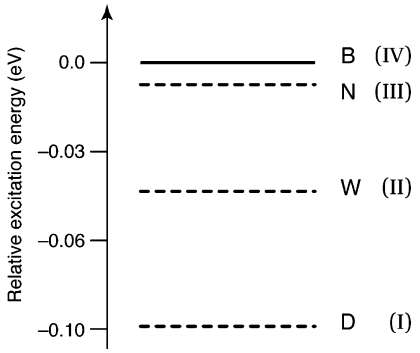

Figure 10. Summary of the lower exciton states that are consistent with interpretation if experimental data.

definitive explanation for why W is weakly allowed. We located the energy of W relative to B by modeling the relative intensities of B and W at various temperatures. Kinetics are explicitly considered, which in conjunction with the detailed balance condition allow us to determine the relative position of W. Our results suggest that the dark state D lies several tens of milli-electrovolts below the bright state, and it merely acts as a population sink, lowering the overall quantum yield for emission, while the W and N dark states control the population dynamics. We note that this assignment is a controversial result, since in other work it has been suggested that D lies only a few milli-electrovolts below B. Our conclusion comes as a consequence of explicitly considering the entire manifold of low-lying exciton bands.

On the other hand, to understand the temperature dependence of B emission only (rather than relative to W), it is likely that a dark state (N, probably exciton band III) lying closely below B is important. The reasoning is similar to that put forward by Mortimer and Nicholas,[60] who assigned the state as D. According to our simulations, it is not a requisite that this state borrows intensity from B, unlike that model because our results suggest that kinetics are important in deciding the depopulation and repopulation of B in concert with the detailed balance condition that fixes the reverse rate relative the depopulation of B. Hence, an important conclusion of our studies is that the rates of interconversion among the low-lying excitons states are significant in dictating models for the photophysics (i.e., the rates cannot be assumed fast such that a Boltzmann distribution of population is rapidly attained). Direct funneling of the population of N to D may well be important in deciding the fluorescence decay kinetics (specifically, the amplitudes of the exponential factors), as well as the observed low quantum yield. Indeed, investigations of the ultrafast dynamics of SWNTs[15,26,27,83] show that relaxation pathways are complicated. We note recent examples of tubular molecular aggregates that also show complicated ultrafast relaxation dynamics,[84,85] highlighting the more general complexity of macromolecular systems.

Overall, our results suggest that the multiple exciton levels located near the E_{11} energy play important roles in dictating experimental observables. The picture we suggest for the lowest exciton states is summarized in Figure 10. The photophysics of SWNTs result from an interplay between radiationless transitions among all four low-lying exciton states, but relaxation within each exciton band appears to be rapid, as assumed in eq 4 and supported by the model simulations in Figure 9b.

Finally, we speculate on the consequences of quenching of the SWNT excitons by trap states. Those traps could be tube ends, chemical impurities bound to the surface, or bonding defects, often known as X traps.[86] The ensemble measurements see an average picture of those processes. Single tube measurements would see a distribution of fluorescence decay times, where the subnanosecond decay time would vary according to the quenching rate k_{nr}^{B} for each tube. That is consistent with experimental observations.[87]

8. Conclusions

In recent work, we reported the observation of dual fluorescence peaks for certain chiral SWNTs. In the present work, we modeled the fluorescence spectra and decay curves as a function of temperature and formulated an effective three-state kinetic model. Complementing that analysis, we reported quantum chemical calculations of the electronic states of the (7,6) and the (7,5) SWNTs. These calculations indicated that there are four important lower exciton bands (I−IV), consistent with previous reports. The lowest (I) is dark, while the upper (IV) is bright, as is by now well-established by other workers. In the present work, we focused on the possible roles played by up to four exciton states at around the E_{11} energy. Analysis based on both frequency and time-domain data provided constraints by which to test various models. Importantly, we found that nonradiative relaxation among the lower exciton bands is not rapid but occurs on time scales of tens to hundreds of picoseconds. In other words, a Boltzmann population distribution among these lower exciton bands is not established prior to radiative decay; thus, Kasha's rule is not obeyed. Kinetics therefore significantly influences the observed photophysics. On the other hand, our model assumes that intraband relaxation is rapid. That model allowed us to explain quantitatively the observation of dual fluorescence bands, even at temperatures as low as 4 K, as well as the fluorescence decay profiles. It is not apparent, however, why the lower energy state is weakly allowed. A challenge for elucidating the photophysical parameters for semiconducting SWNTs is to account for the temperature-dependent radiative rates of each band. We found evidence to suggest that this effect is more significant than the temperature-dependence of the nonradiative rates. Overall, we conclude that, to understand and to interpret the low quantum yield of emission and the decay dynamics, a kinetic model that captures the nonradiative relaxation among the lower exciton states is essential.

Acknowledgment. This work was funded by the U.S. Department of Energy's Solar Photochemistry Program within the Office of Science, Office of Basic Energy Sciences, Division of Chemical Sciences, Geosciences, and Biosciences and NSERC Canada. GDS thanks the Alfred P. Sloan Foundation. The research at LANL is supported by Center for Integrated Nanotechnology (CINT), Center for Nonlinear Studies (CNLS), and the OBES program of the U.S. Department of Energy.

References and Notes

(1) Ando, T. *J. Phys. Soc. Jpn.* **1997**, *66*, 1066.

(2) Bachilo, S. M.; Strano, M. S.; Kittrell, C.; Hauge, R. H.; Smalley, R. E.; Weisman, R. B. *Science* **2002**, *298*, 2361.

(3) Cohen, M. L. *Mater. Sci. Eng., C* **2001**, *15*, 1.

(4) O'Connell, M. J.; Bachilo, S. M.; Huffman, C. B.; Moore, V. C.; Strano, M. S.; Haroz, E. H.; Rialon, K. L.; Boul, P. J.; Noon, W. H.; Kittrell, C.; Ma, J.; Hauge, R. H.; Weisman, R. B.; Smalley, R. E. *Science* **2002**, *297*, 593.

(5) Reich, S.; Thomsen, C.; Maultzsch, J. *Carbon nanotubes: Basic concepts and physical properties*; Wiley: New York, 2004.

(6) Dresselhaus, M. S.; Dresselhaus, G.; Saito, R.; Jorio, A. *Phys. Rep.* **2005**, *409*, 47.

(7) Zhao, H.; Mazumdar, S.; Sheng, C.-X.; Tong, M.; Vardeny, Z. V. *Phys. Rev. B* **2006**, *73*, 75403.

(8) Sfeir, M. Y.; Beetz, T.; Wang, F.; Huang, L.; Huang, X. M. H.; Huang, M.; Hone, J.; O'Brien, S.; Misewich, J. A.; Heinz, T. F.; Wu, L.; Zhu, Y.; Brus, L. E. *Science* **2006**, *312*, 554.

(9) Hartschuh, A.; Pedrosa, H. N.; Novotny, L.; Krauss, T. D. *Science* **2003**, *301*, 1354.

(10) Htoon, H.; O'Connell, M. J.; Doorn, S. K.; Klimov, V. I. *Phys. Rev. Lett.* **2005**, *94*, 127403.

(11) Scholes, G. D.; Rumbles, G. *Nat. Mater.* **2006**, *5*, 683.

(12) Spataru, C. D.; Ismail-Beigi, S.; Benedict, L. X.; Louie, S. G. *Phys. Rev. Lett.* **2004**, *92*, 77402.

(13) Zhao, H.; Mazumdar, S. *Phys. Rev. Lett.* **2004**, *93*, 157402.

(14) Wang, F.; Dukovic, G.; Brus, L. E.; Heinz, T. F. *Science* **2005**, *308*, 838.

(15) Ma, Y.-Z.; Valkunas, L.; Bachilo, S. M.; Fleming, G. R. *J. Phys. Chem. B* **2005**, *109*, 15671.

(16) Chang, E.; Bussi, G.; Ruini, A.; Molinari, E. *Phys. Rev. Lett.* **2004**, *92*, 196401.

(17) Kane, C. L.; Mele, E. J. *Phys. Rev. Lett.* **2004**, *93*, 197402.

(18) Spataru, C. D.; Ismail-Beigi, S.; Capaz, R. B.; Louie, S. G. *Phys. Rev. Lett.* **2005**, *95*, 247402.

(19) Perebeinos, V.; Tersoff, J.; Avouris, P. *Nano Lett.* **2005**, *5*, 2495.

(20) Jones, M.; Engtrakul, C.; Metzger, W. K.; Ellingson, R. J.; Nozik, A. J.; Heben, M. J.; Rumbles, G. *Phys. Rev. B* **2005**, *71*, 115426.

(21) Kasha, M. *Discuss. Faraday Soc.* **1950**, 14.

(22) Kasha, M.; McGlynn, S. P. *Annu. Rev. Phys. Chem.* **1956**, *7*, 403.

(23) Metzger, W. K.; McDonald, T. J.; Engtrakul, C.; Blackburn, J. L.; Scholes, G. D.; Rumbles, G.; Heben, M. J. *J. Phys. Chem. C* **2007**, *111*, 3601.

(24) Karaiskaj, D.; Engtrakul, C.; McDonald, T.; Heben, M. J.; Mascarenhas, A. *Phys. Rev. Lett.* **2006**, *96*, 106805.

(25) McDonald, T.; Jones, M.; Engtrakul, C.; Ellingson, R. J. *Rev. Sci. Instrum.* **2006**, *77*, 53104.

(26) Valkunas, L.; Ma, Y.-Z.; Fleming, G. R. *Phys. Rev. B* **2006**, *73*, 115432.

(27) Ellingson, R. J.; Engtrakul, C.; Jones, M.; Samec, M.; Rumbles, G.; Nozik, A. J.; Heben, M. J. *Phys. Rev. B* **2005**, *71*, 115444.

(28) Frisch, M. J.; Trucks, G. W.; Schlegel, H. B.; Scuseria, G. E.; Robb, M. A.; Cheeseman, J. R.; Montgomery, J. A., Jr.; Vreven, T.; Kudin, K. N.; Burant, J. C.; Millam, J. M.; Iyengar, S. S.; Tomasi, J.; Barone, V.; Mennucci, B.; Cossi, M.; Scalmani, G.; Rega, N.; Petersson, G. A.; Nakatsuji, H.; Hada, M.; Ehara, M.; Toyota, K.; Fukuda, R.; Hasegawa, J.; Ishida, M.; Nakajima, T.; Honda, Y.; Kitao, O.; Nakai, H.; Klene, M.; Li, X.; Knox, J. E.; Hratchian, H. P.; Cross, J. B.; Bakken, V.; Adamo, C.; Jaramillo, J.; Gomperts, R.; Stratmann, R. E.; Yazyev, O.; Austin, A. J.; Cammi, R.; Pomelli, C.; Ochterski, J. W.; Ayala, P. Y.; Morokuma, K.; Voth, G. A.; Salvador, P.; Dannenberg, J. J.; Zakrzewski, V. G.; Dapprich, S.; Daniels, A. D.; Strain, M. C.; Farkas, O.; Malick, D. K.; Rabuck, A. D.; Raghavachari, K.; Foresman, J. B.; Ortiz, J. V.; Cui, Q.; Baboul, A. G.; Clifford, S.; Cioslowski, J.; Stefanov, B. B.; Liu, G.; Liashenko, A.; Piskorz, P.; Komaromi, I.; Martin, R. L.; Fox, D. J.; Keith, T.; Al-Laham, M. A.; Peng, C. Y.; Nanayakkara, A.; Challacombe, M.; Gill, P. M. W.; Johnson, B.; Chen, W.; Wong, M. W.; Gonzalez, C.; Pople, J. A. *Gaussian 03*, revision D.02; Gaussian, Inc.: Wallingford, CT, 2004.

(29) Becke, A. D. *J. Chem. Phys.* **1993**, *98*, 5648.

(30) Perdew, J. P.; Burke, K.; Emzerhof, M. *Phys. Rev. Lett.* **1996**, *77*, 3865.

(31) Tretiak, S.; Igumenshchev, K.; Chernyak, V. *Phys. Rev. B* **2005**, *71*, 33201.

(32) Onida, G.; Reining, I.; Rubio, A. *Rev. Mod. Phys.* **2002**, *74*, 601.

(33) Masunov, A. M.; Tretiak, S. *J. Phys. Chem. B* **2004**, *108*, 899.

(34) Jha, P. C.; Jansson, E.; Agren, H. *Chem. Phys. Lett.* **2006**, *424*, 23.

(35) Zhou, Z. Y.; Steigerwald, M.; Hybertsen, M.; Brus, L. E.; Friesner, R. A. *J. Am. Chem. Soc.* **2004**, *126*, 3597.

(36) Tretiak, S. *Nano Lett.* **2006**, in press.

(37) Brédas, J. L.; Cornil, J.; Beljonne, D.; dos Santos, D. A.; Shuai, Z. *Acc. Chem. Res.* **1999**, *32*, 267.

(38) Tretiak, S.; Mukamel, S. *Chem. Rev.* **2002**, *102*, 3171.

(39) Tretiak, S.; Saxena, A.; Martin, R. L.; Bishop, A. R. *Phys. Rev. Lett.* **2002**, *89*, 97402.

(40) Gambetta, A.; Manzoni, C.; Meneghetti, M.; Cerullo, G.; Lanzani, G.; Tretiak, S.; Piryatinski, A.; Saxena, A.; Martin, R. L.; Bishop, A. R. *Nature, Phys. Sci.* **2006**, *2*, 515.

(41) Tretiak, S.; Kilina, S.; Piryatinski, A.; Saxena, A.; Martin, R. L.; Bishop, A. R. *Nano Lett.* **2007**, *7*, 86−92.

(42) Shreve, A. P.; Haroz, E. H.; Bachilo, S. M.; Weisman, R. B.; Tretiak, S.; Kilina, S.; Doorn, S. K. *Phys. Rev. Lett.* **2007**, *98*, 037405.

(43) Jorio, A.; Fantani, C.; Pimenta, M. A.; Capaz, R. B.; Samsonidze, G. G.; Dresselhaus, G.; Dresselhaus, M. S.; Jiang, J.; Kobayashi, N.; Grüneis, A.; Saito, R. *Phys. Rev. B* **2005**, *71*, 75401.

(44) Guha, S.; Rice, J. D.; Yau, Y. T.; Martin, C. M.; Chandrasekhar, M.; Chandrasekhar, H. R.; Guentner, R.; Scanduicci de Freitas, P.; Scherf, U. *Phys. Rev. B* **2003**, *67*, 125204.

(45) Gierschner, J.; Cornil, J.; Egelhaaf, H.-J. *Adv. Mater.* **2007**, *19*, 173−191.

(46) Perebeinos, V.; Tersoff, J.; Avouris, P. *Phys. Rev. Lett.* **2004**, *92*, 257402.

(47) Andersson, K.; Roos, B. O. *Int. J. Quantum Chem.* **1993**, *45*, 591.

(48) Serranoandres, L.; Merchan, M.; Nebotgil, I.; Lindh, R.; Roos, B. O. *J. Chem. Phys.* **1993**, *98*, 3151.

(49) Li, X. Z.; Paldus, J. *J. Chem. Phys.* **2004**, *120*, 5890.

(50) Dreuw, A.; Head-Gordon, M. *Chem. Rev.* **2005**, *105*, 4009.

(51) Cronstrand, P.; Christiansen, O.; Norman, P.; Ågren, H. *Phys. Chem. Chem. Phys.* **2001**, *3*, 2567.

(52) Wang, Z.; Zhao, H.; Mazumdar, S. *Phys. Rev. B* **2006**, *74*, 195406.

(53) Wu, C.; Malinin, S.; Tretiak, S.; Chernyak, V. *Nature, Phys. Sci.* **2006**, *2*, 631.

(54) Beljonne, D.; Shuai, Z.; Cornil, J.; dos Santos, D. A.; Brédas, J. L. *J. Chem. Phys.* **1999**, *111*, 2829.

(55) Barros, E. B.; Capaz, R. B.; Jorio, A.; Samsonidze, G. G.; Souza Filho, A. G.; Ismail-Beigi, S.; Spataru, C. D.; Louie, S. G.; Dresselhaus, G.; Dresselhaus, M. S. *Phys. Rev. B* **2006**, *73*, 241406.

(56) Martin, R. L. *J. Chem. Phys.* **2003**, *118*, 4775.

(57) Ando, T. *J. Phys. Soc. Jpn.* **2006**, *75*, 024707.

(58) Didraga, C.; Knoester, J. *Chem. Phys.* **2002**, *275*, 307.

(59) Zaric, S.; Ostojic, G. N.; Kono, J.; Shaver, J.; Moore, V. C.; Strano, M. S.; Hauge, R. H.; Smalley, R. E.; Wei, X. *Science* **2004**, *304*, 1129.

(60) Mortimer, I. B.; Nicholas, R. J. *Phys. Rev. Lett.* **2007**, *98*, 027404.

(61) Herzberg, G. *Electronic spectra and electronic structure of polyatomic molecules*; Van Nostrand: Princeton, New Jersey, 1967.

(62) Murrell, J. N.; Pople, J. A. *Proc. Phys. Soc., London* **1956**, *69*, 245.

(63) Reber, C.; Yee, L.; McKiernan, J.; Zink, J. I.; Williams, R. S.; Tong, W. M.; Ohlberg, D. A. A.; Whetten, R. L.; Diederich, F. *J. Phys. Chem.* **1991**, *95*, 2127.

(64) Vukovic, T.; Milosevic, I.; Damnjanovic, M. *Phys. Rev. B* **2002**, *65*, 45418.

(65) Robinson, G. W. *J. Chem. Phys.* **1967**, *46*, 572.

(66) van Strien, A. J.; Schmidt, J.; Silbey, R. *Mol. Phys.* **1982**, *46*, 151.

(67) Lin, S. H.; Bersohn, R. *J. Chem. Phys.* **1968**, *48*, 2732.

(68) Lin, S. H. *J. Chem. Phys.* **1972**, *56*, 2648.

(69) Fidder, H.; Terpstra, J.; Wiersma, D. A. *J. Chem. Phys.* **1991**, *94*, 6895.

(70) Kamalov, V. F.; Struganova, I. A.; Yoshihara, K. *J. Phys. Chem.* **1996**, *100*, 8640.

(71) Bednarz, M.; Malyshev, V. A.; Knoester, J. *Phys. Rev. Lett.* **2003**, *91*, 217401.

(72) Bednarz, M.; Malyshev, V. A.; Knoester, J. *J. Chem. Phys.* **2002**, *117*, 6200.

(73) Myers, A. B. *Chem. Phys.* **1994**, *180*, 215.

(74) Mukamel, S. *Principles of nonlinear optical spectroscopy*; Oxford Univesity Press: New York, 1995.

(75) Fleming, G. R.; Passino, S. A.; Nagasawa, Y. *Philos. Trans. R. Soc. London, Ser. A* **1998**, *356*, 389.

(76) Lawrence, C. P.; Skinner, J. L. *Proc. Natl. Acad. Sci. U.S.A.* **2005**, *102*, 6720.

(77) Bader, J. S.; Berne, B. J. *J. Chem. Phys.* **1994**, *100*, 8359.

(78) Arnold, K.; Lebedkin, S.; Kiowski, O.; Hennrich, F.; Kappes, M. M. *Nano Lett.* **2004**, *4*, 2349.

(79) Nakajima, S. *The physics of elementary excitations*; Springer-Verlag: New York, 1980.

(80) Jones, M.; Metzger, W. K.; McDonald, T. J.; Engtrakul, C.; Ellingson, R. J.; Rumbles, G.; Heben, M. J. *Nano Lett.* **2007**, *7*, 300−306.

(81) Birks, J. B. *Photophysics of aromatic molecules*; Wiley: New York, 1970.

(82) Miller, P. F.; de Souza, M. M.; Moratti, S. C.; Holmes, A. B.; Samuel, I. D. W.; Rumbles, G. *Polym. Int.* **2006**, *55*, 784.

(83) Seferyan, H. Y.; Nasr, M. B.; Senekerimyan, V.; Zadoyan, R.; Collins, P.; Apkarian, V. A. *Nano Lett.* **2006**, *6*, 1757.

(84) Pugzlys, A.; Augulis, R.; van Loosdrecht, P. H. M.; Didraga, C.; Malyshev, V. A.; Knoester, J. *J. Phys. Chem. B* **2006**, *110*, 20268.

(85) Augulis, R.; Pugzlys, A.; van Loosdrecht, P. H. M. *Phys. Status Solidi C* **2006**, *3*, 3400.

(86) Guss, W.; Feldmann, J.; Göbel, E. O.; Taliani, C.; Mohn, H.; Müller, W.; Häussler, P.; ter Meer, H.-U. *Phys. Rev. Lett.* **1994**, *72*, 2644.

(87) Hagen, A.; Steiner, M.; Raschke, M. B.; Lienau, C.; Hertel, T.; Qian, H.; Meixner, A. J.; Hartschuh, A. *Phys. Rev. Lett.* **2005**, *95*, 197401.